

# Explicit Algebraic Reynolds Stress Models for Anisotropic Wall-Bounded Flows

F. R. Menter<sup>1</sup>, A. V. Garbaruk<sup>2</sup> and Y. Egorov<sup>1</sup>

<sup>1</sup> ANSYS Germany GmbH, Germany

<sup>2</sup> NTS St. Petersburg, Russia

## Introduction

Current industrial and aeronautics CFD simulations are largely based on linear eddy-viscosity turbulence models (LEVM). There are several reasons why higher order models like Reynolds Stress Models (RSM) have rarely made their way into mainstream industrial CFD applications, even though they are available in most general-purpose codes. The two main reasons are the increased computational requirements, often caused by a lack of robustness and the observation that such models have in many cases not resulted in a systematic improvement of results. Still there are numerous areas where EV models are known to fail systematically and where further model improvements are required. The goal should be to allow the inclusion of specific additional effects without a large penalty on speed and robustness.

Explicit Algebraic RSM (EARSM) (Pope, 1975, Rodi, 1976, Gatski and Speziale, 1993, Wallin and Johansson, 2000) offer an attractive framework for such enhancements. These models can be considered as a subset of nonlinear constitutive relations in which a part of the higher-order description of physical processes on the RSM-level is transferred into the two-equation modeling level. As a result, they are much less demanding than RSM from the computational standpoint and, at the same time, are capable of reproducing some important features of turbulence (e.g. its anisotropy in the normal stresses), which are beyond the capabilities of LEVM. The emphasis in the development of EARSM has largely been on the correct mathematical formulation of the stress-strain relationship and not so much in the formulation of an industrial CFD model (see however Hellsten and Laine, 2000).

When increasing the complexity in the formulation of a turbulence model, one should first answer the question, which types of flows will benefit from it? One of the weaknesses of EARSMs is that they do not naturally account for swirling and rotating flows. This being one of the major practical arguments for RSM, one has to find other areas where EARSM could be beneficial (or add appropriate rotation terms). One such area is the prediction of flows parallel to corners formed by intersecting walls, as observed in wing-body junctions or hub-blade regions. There is a strong indication that LEVM predict much too early separation from such corners when the flow is exposed to adverse pressure gradients. This can have a severe impact on the computed performance characteristics of these technical devices. The goal of the current paper is to explore model enhancements which allow the inclusion of such effects at the lowest level of complexity. For this purpose, two EARSM formulations will be investigated. The underlying idea being that the secondary flow of the

second kind which is observed near corners is the main mechanism for obtaining delayed separation in these regions. In other words, it is anticipated that the secondary flow caused by the differences in the normal stresses drives additional momentum into the corner, thereby delaying separation. The goal is the identification of the most appropriate and simplest EARSM formulation which allows the inclusion of anisotropic effects into the formulation. There are two areas which will be investigated.

The first is the formulation of a scale-equation used in combination with the EARSM. Experience over the last decade has shown that  $\omega$ -equation based models offer significant advantages over  $\varepsilon$ -equation based models, especially if integration through the viscous sublayer is desired (Menter, 2009). Unfortunately, the standard  $\omega$ -equation of Wilcox in its different forms is not suitable due to the persistent freestream sensitivity of this model, even in its latest version (Menter, 2004, 2009). In addition, the Shear Stress Transport (SST) model (Menter, 1994) has been widely used in aerodynamic and other industrial flow simulations. It is therefore desirable to formulate the EARSM on the basis of a scale-equation very similar to the SST model in order to isolate the impact of the stress-strain relationship on the solution. The starting point is therefore the Baseline (BSL) model, which underlies the SST model (Menter, 1994). It will be shown that an EARSM can be formulated without a need for re-calibrating the BSL model. This allows the direct comparison of the EARSM stress-strain relationship with the SST model formulation, without additional changes of other parts of the model.

The second area of interest is the formulation of the non-linear stress-strain relationship. Here, numerous options are available in the literature and can be used as a starting point. Starting point in this paper is the stress-strain relation proposed by Wallin and Johansson (1997, 2000) (WJ) which already provides a relatively simple EARSM closure. In addition, the question is posed: “what is the simplest EARSM which would still account for the anisotropy in the normal stresses in wall-bounded flows?” and would thereby allow the prediction of secondary flow into the corner. A model variant is explored which is linear in the implicit formulation, resulting in a simplification of the WJ stress-strain relation.

The models are tested for a set of flows with an emphasis of corner flow behavior. In addition, a flat plate boundary layer will be shown to demonstrate that the model gives the correct wall shear stress and log. boundary layer profile. In some of the testcases, a comparison with the SST model is given. It should be emphasized that the superior performance for some of the corner flow cases does not imply a general recommendation for replacing the SST with the EARSM at current point. For such a recommendation, significantly more testing and model optimization (especially in terms of robustness) is required.

## **Model Formulation**

### **The Wallin-Johansson Stress-Strain Relationship**

The starting point for the current investigation is the EARSM formulation of Wallin and Johansson (2000). The main contribution of WJ lies in a compact formulation of an EARSM based on a slightly simplified Launder-Reece-Rodi RSM. In the framework of this model the anisotropy tensor,  $a_{ij}$ , defined through the Reynolds stress tensor  $\tau_{ij}$

$$\tau_{ij} = \overline{u'_i u'_j} = k \left( a_{ij} + \frac{2}{3} \delta_{ij} \right) \quad (1)$$

is decomposed into a tensor basis as follows

$$a_{ij} = \beta_1 T_{1,ij} + \beta_2 T_{2,ij} + \beta_3 T_{3,ij} + \beta_4 T_{4,ij} + \beta_6 T_{6,ij} + \beta_9 T_{9,ij} \quad (2)$$

where

$$\begin{aligned} T_{1,ij} &= S_{ij}; T_{2,ij} = S_{ik} S_{kj} - \frac{1}{3} II_S \delta_{ij}; T_{3,ij} = \Omega_{ik} \Omega_{kj} - \frac{1}{3} II_\Omega \delta_{ij}; T_{4,ij} = S_{ik} \Omega_{kj} - \Omega_{ik} S_{kj} \\ T_{6,ij} &= S_{ik} \Omega_{kl} \Omega_{lj} + \Omega_{ik} \Omega_{kl} S_{lj} - \frac{2}{3} IV \delta_{ij} - II_\Omega S_{ij}; \\ T_{9,ij} &= \Omega_{ik} S_{kl} \Omega_{lm} \Omega_{mj} - \Omega_{ik} \Omega_{kl} S_{lm} \Omega_{mj} + \frac{1}{2} II_\Omega (S_{ik} \Omega_{kj} - \Omega_{ik} S_{kj}) \end{aligned} \quad (3)$$

The quantities  $S_{ij}$ , and  $\Omega_{ij}$  in (3) are the non-dimensional strain and vorticity tensors of the mean flow

$$S_{ij} = \frac{\tau}{2} \left( \frac{\partial U_i}{\partial x_j} + \frac{\partial U_j}{\partial x_i} \right), \quad \Omega_{ij} = \frac{\tau}{2} \left( \frac{\partial U_i}{\partial x_j} - \frac{\partial U_j}{\partial x_i} \right) \quad (4)$$

where  $\tau$ , is the time scale with a Kolmogorov limiter (Durbin, 1991)

$$\tau = \max \left( \frac{1}{C_\mu \omega}, 6 \cdot \sqrt{\frac{\nu}{C_\mu k \omega}} \right) \quad (5)$$

and the tensor invariants  $II_S$ ,  $II_\Omega$  and  $IV$  read as

$$II_S = S_{ij} S_{ji}, \quad II_\Omega = \Omega_{ij} \Omega_{ji}, \quad IV = S_{ik} \Omega_{kj} \Omega_{ji} \quad (6)$$

The coefficients of the tensor basis  $\beta_i$  in (2) are defined as:

$$\beta_1 = -\frac{N}{Q}, \quad \beta_2 = 0, \quad \beta_3 = -\frac{2IV}{NQ_1}, \quad \beta_4 = -\frac{1}{Q}, \quad \beta_6 = -\frac{N}{Q_1}, \quad \beta_9 = \frac{1}{Q_1} \quad (7)$$

with

$$Q = \frac{(N^2 - 2II_\Omega)}{A_1}, \quad Q_1 = \frac{Q}{6} (2N^2 - II_\Omega) \quad (8)$$

where

$$N = C'_1 + \frac{9}{4} \frac{P_k}{\varepsilon} \quad (9)$$

$$A_1 = 1.2 \quad \text{and} \quad C'_1 = \frac{9}{4} (C_1 - 1), \quad C_1 = 1.8$$

where  $N$  is a solution of the cubic equation

$$N^3 - C_1' N^2 - (2.7 \cdot II_s + 2 \cdot II_\Omega) N + 2C_1' II_\Omega = 0 \quad (10)$$

which is given by:

$$\begin{cases} N = \frac{C_1'}{3} + (P_1 + \sqrt{P_2})^{1/3} + \text{sign}(P_1 - \sqrt{P_2}) |P_1 - \sqrt{P_2}|^{1/3} & \text{at } P_2 \geq 0 \\ N = \frac{C_1'}{3} + 2(P_1^2 - P_2)^{1/6} \cos\left(\frac{1}{3} \arccos\left(\frac{P_1}{\sqrt{P_1^2 - P_2}}\right)\right) & \text{at } P_2 < 0 \end{cases} \quad (11)$$

with

$$P_1 = C_1' \left( \frac{C_1'^2}{27} + \frac{9}{20} II_s - \frac{2}{3} II_\Omega \right), \quad P_2 = P_1^2 - \left( \frac{C_1'^2}{9} + \frac{9}{10} II_s + \frac{2}{3} II_\Omega \right)^3 \quad (12)$$

### The BSL-EARSM

The WJ stress-strain relationship above was originally combined with the  $k$ - $\omega$  equations as given by Wilcox (Wallin and Johansson, 2000). In order to avoid the freestream sensitivity of the Wilcox model, the WJ stress-strain relation is combined here with the BSL  $k$ - $\omega$  model (Menter, 1994). To avoid a re-calibration or the need for additional terms in the BSL model, a slight re-calibration of the WJ-EARSM was performed, namely a 4% increase of the  $A_I=1.245$  parameter (instead of  $A_I=1.2$  in WJ Eq. 8-9) (Wallin, 2009). This allows matching the logarithmic wall layer without changing the EARSM stress-strain relationship. It is also important to point out that the eddy-viscosity used in the diffusion terms of the  $k$ - and  $\omega$ -equations is computed from:  $\nu_t = k/\omega$ . This choice avoids the problems observed and resolved by Hellsten and Laine (2000) near the boundary layer edge.

The complete BSL-EARSM reads:

$$\begin{cases} \frac{Dk}{Dt} = \nabla \cdot ((\nu + \sigma_k \nu_t) \nabla k) + \tilde{P}_k - \beta^* k \omega \\ \frac{D\omega}{Dt} = \nabla \cdot ((\nu + \sigma_\omega \nu_t) \nabla \omega) + \frac{\gamma \omega}{k} \tilde{P}_k - \beta \omega^2 + \frac{\sigma_d}{\omega} (\nabla k) \cdot (\nabla \omega) \end{cases}, \quad (13)$$

where  $P_k$  is given by (using a production limiter as in the SST model):

$$\tilde{P}_k = \min\left(-\tau_{ij} \frac{\partial U_i}{\partial x_j}, 10 \cdot \rho \beta^* k \omega\right) \quad (14)$$

The model constants are defined via the corresponding constants of the  $k$ - $\varepsilon$  (subscript “1”) and  $k$ - $\omega$  (subscript “2”) branches of the BSL model with the use of the blending function  $F_1$ .

$$\sigma_k = F_1 \sigma_{k1} + (1 - F_1) \sigma_{k2}, \sigma_\omega = F_1 \sigma_{\omega1} + (1 - F_1) \sigma_{\omega2}, \beta = F_1 \beta_1 + (1 - F_1) \beta_2, \sigma_d = 2(1 - F_1) \sigma_{\omega2}$$

$$\sigma_{k1} = 0.5, \sigma_{k2} = 1.0, \sigma_{\omega1} = 0.5, \sigma_{\omega2} = 0.856, \beta_1 = 0.075, \beta_2 = 0.0828, \beta^* = C_\mu = 0.09, \gamma = \frac{\beta}{\beta^*} - \frac{\sigma_\omega \kappa^2}{\sqrt{\beta^*}}.$$

where the function  $F_1$  reads as ( $d$  is the distance to the nearest wall)

$$F_1 = \tanh(\arg_1^4), \quad \arg_1 = \min \left[ \max \left( \frac{\sqrt{k}}{C_\mu \omega d}, \frac{500\nu}{\omega d^2} \right), \frac{2k\omega}{d^2 (\nabla k) \cdot (\nabla \omega)} \right] \quad (15)$$

Note that the model does not include the term  $T_{9,ij}$  ( $\beta_9 = 0$ ): as was shown by the preliminary computations, this term does not cause any visible alteration of the obtained solution.

### The simplified BSL-EARSM (S-BSL-EARSM)

In order to explore the most simplified EARSM formulation which would still allow the inclusion of near wall normal stress anisotropies, the formulation of WJ was simplified in the non-linear portion of the model. The non-linearity in the implicit ARSM results from the production term  $P_k$ , which again contains the unknown Reynolds Stresses (or anisotropies). A simplified formulation can be obtained by replacing the ratio of production/dissipation in (9) by the following equilibrium assumption (similar to the SST assumption):

$$\frac{P_k}{\varepsilon} = \sqrt{2C_\mu II_S} \quad (16)$$

This results in a linear formulation for the quantity  $N$  instead of (10)-(12):

$$N = C'_1 + \frac{9}{4} \frac{P_k}{\varepsilon} = C'_1 + \frac{9}{4} \sqrt{2C_\mu II_S}. \quad (17)$$

The rest of the model formulation remains unchanged. The hope of this simplification is to improve the robustness of the model by reducing its non-linearities. This is intended as a test of model variants. It is clear that generality is sacrificed by this simplification, but for the goal of computing corner separation in wall boundary layer flows, the assumption seems justified.

### Flow Solver

The above models have been implemented into a prototype version of the ANSYS-CFX-12 solver and an in-house code of NTS (Strelets, 2001). Cross-validation of the codes with successive grid refinement for all testcases has shown that the model implementation is code independent.

# Testcases

## Flat Plate Boundary Layer

The first tests were carried out for a flat plate boundary layer with zero pressure gradient. The simulations are compared against experimental data of Wieghart and Tillmann (1951). Three meshes were used in the tests to ensure grid independence. The grids are all of resolution with  $y^+ < 1$ . Figure 1 shows the wall shear stress distribution  $c_f$  and the velocity profile in a logarithmic scale. For both plots the new models (BSL-EARSM, S-BSL-EARSM) agree well with the data.

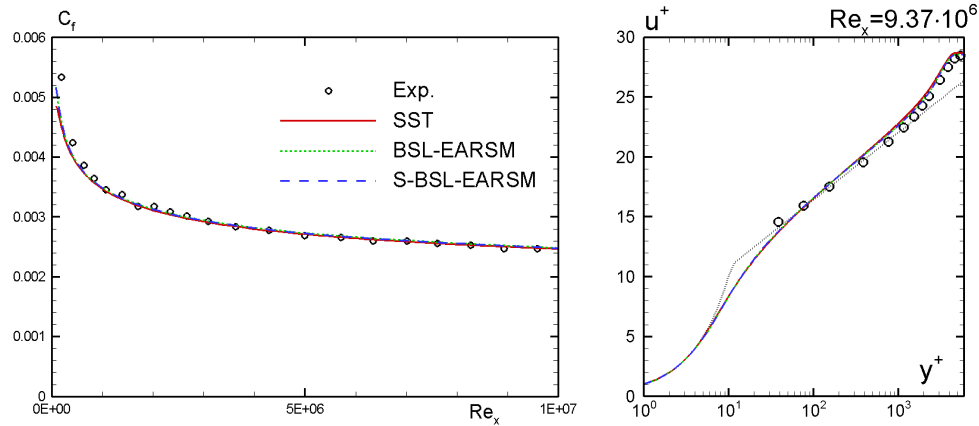


Figure 1: Comparison of skin-friction coefficient distributions and velocity profiles in a flat plate boundary layer computed with the use of different EARSM and SST model with experimental data of Wieghardt, Tillman, 1951

## 3D Developed Flow in a Square Duct

This testcase represents an example of flows which show an essential influence of the anisotropy of turbulence on the mean flow. In particular, the anisotropy causes the formation of a secondary flow, which is beyond the capabilities of LEVM.

The computations were performed at a Reynolds number based on the mean friction-velocity and the channel half-width,  $h$ , equal to 6000 which corresponds to the conditions of the DNS of Huser and Biringen, (1993).

The computations are carried out in a  $\frac{1}{4}$  quadrant of the whole channel with symmetry conditions imposed at  $y = z = h$ , see Figure 2. At the streamwise boundaries a periodic condition was applied and at the solid walls no-slip conditions were used. The grid in the YZ-plane also shown in the figure has a size of  $51 \times 51$ . It is refined near the solid wall so that the near wall values of  $y^+$  and  $z^+$  are not higher than 0.3.

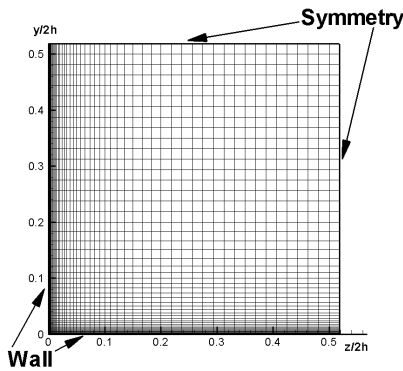


Figure 2: Computational domain and mesh used for computations of the fully developed square duct case.

Figure 3 shows the axial  $u$ -velocity and the  $v$ -velocity normal to the lower wall along a line  $y=z$ . Both EARSM formulations give essentially the same result. The SST model, as all linear eddy-viscosity models (LEVM), predicts a zero value for the  $v$ -velocity, meaning that no secondary flow is produced in the  $y$ - $z$  plane. This is a known deficiency of LEVMs, as the secondary flow is driven by differences in the normal stresses, which cannot be accounted for by LEVMs. Figure 3 (left) shows the main effect of interest in the current study, namely the increased axial momentum transfer into the corner, manifesting itself by a higher axial velocity near the corner walls. It is expected that this effect will help to delay corner separation under adverse pressure gradients. The current comparison is done for a relatively low Reynolds number. Further tests at higher Reynolds numbers are still required.

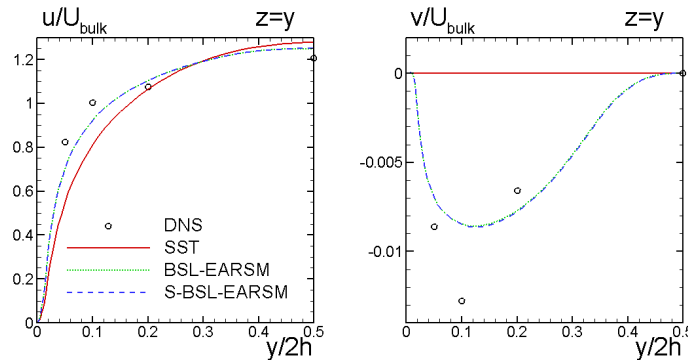


Figure 3: Comparison mean and diametric velocity along line  $y=z$ .

### Incompressible flow in a rectangular diffuser

This flow studied experimentally by Cherry et al. (2007) is a much more challenging testcase than the developed flow considered above. Along with the turbulence anisotropy typical of rectangular channel flows, it involves an adverse pressure gradient causing separation. This separation has proven very sensitive to details of turbulence modeling (ERCOFTAC, 2008). It seems clear that the anisotropy of the normal stresses has to be accounted for in order to avoid the formation of an incorrect flow topology.

The geometry of the diffuser and coordinate system used in the computations are shown in Figure 4. The origin of the coordinate system in the  $x$ -direction is located at the

cross-section of the diffuser corresponding to the intersection of its straight inlet and the inclined walls.

According to the experimental setup, the flow at the diffuser inlet is treated as a fully developed flow in a rectangular duct with the bulk velocity of 1 m/sec. Therefore the velocity in the inlet plane has to be specified based on the precursor computation of the developed duct flow with the use of corresponding (same as that used for the diffuser computation) turbulence model.

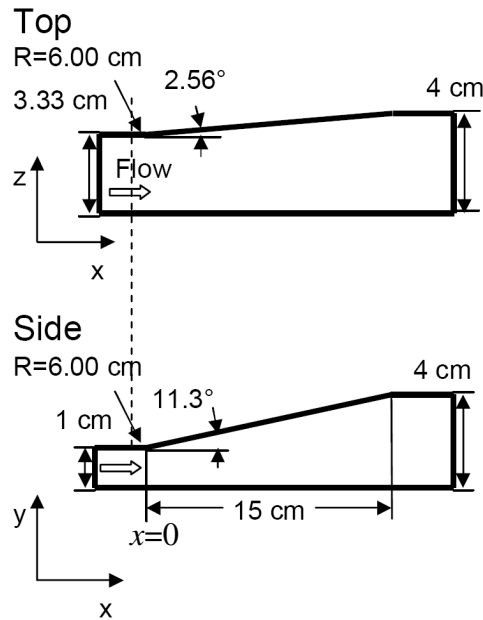


Figure 4: Geometrical of the rectangular diffuser.

Figure 5 presents the computational domain and the mesh used in the computations. It has  $145 \times 91 \times 121$  nodes in the  $x$ ,  $y$  and  $z$  directions respectively and is refined in  $y$ - and  $z$ -directions near all the walls (the maximum value of  $y^+$  is 0.7) and, in the  $x$ -direction, inside the diffuser. The grid for the simulation of the inlet section consists of  $91 \times 121$  nodes.

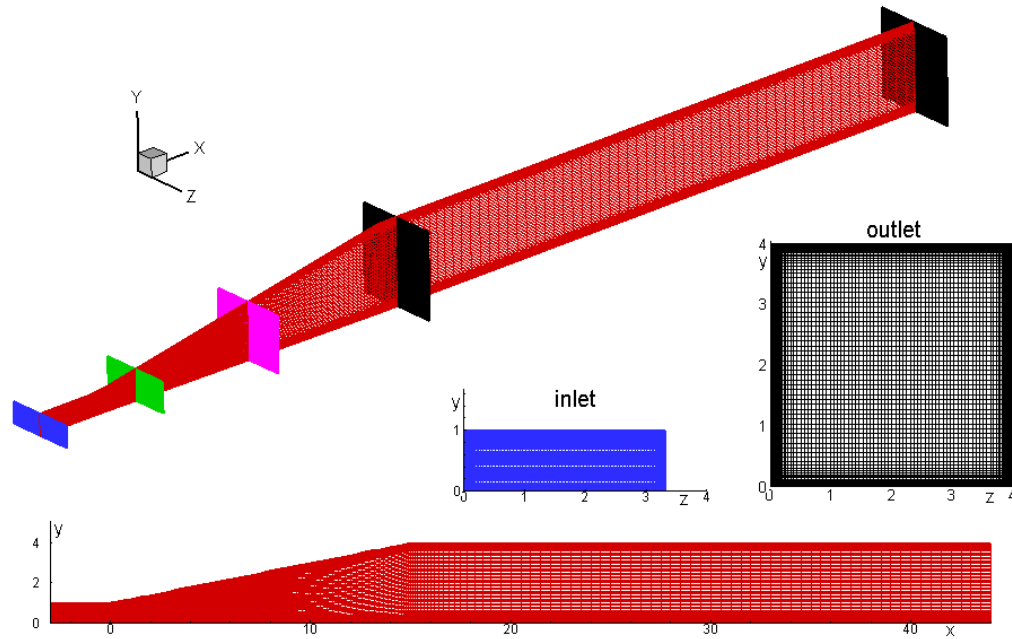


Figure 5: Computational domain and grid used for the rectangular diffuser flow case.

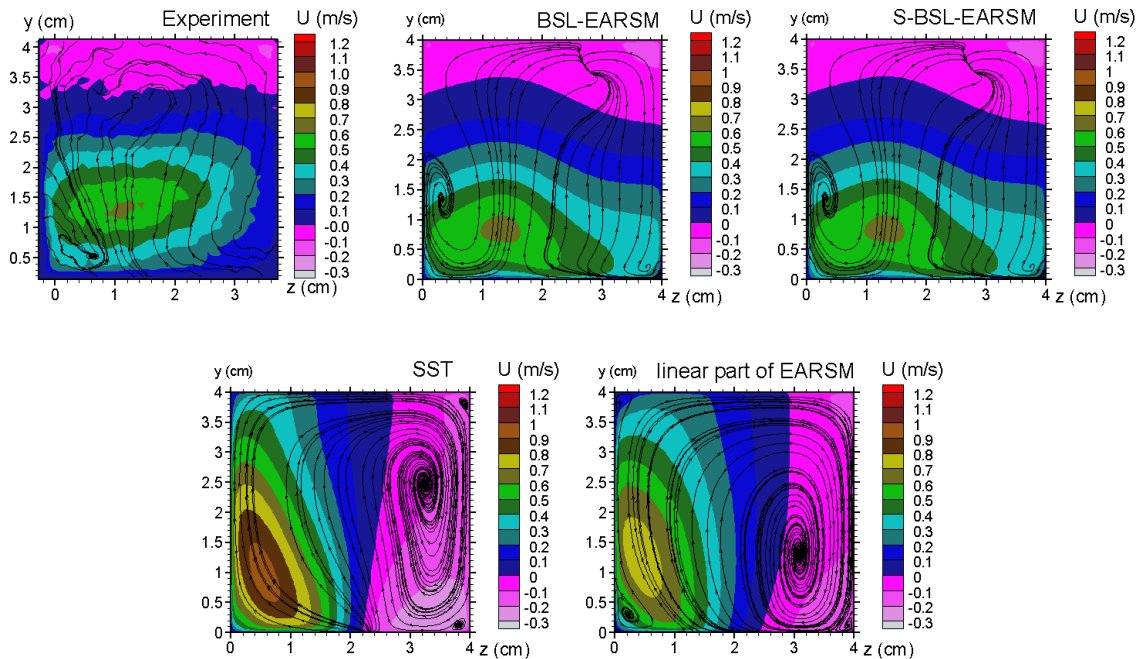


Figure 6: Comparison velocity fields at section  $x=16$  cm.

Figure 6 shows a comparison of the velocity field in the streamwise plane  $x=16$  cm against experimental data. In order to investigate the influence of the anisotropy on the flow, the BSL-EARSM was also run with only the isotropic contribution  $\beta_1 T_1$  (see Eqs. (1-3)) activated. It can be seen that the isotropic contribution of the EARSM and the SST model are not able to predict the correct flow topology. This is the main argument for using anisotropic formulations for such flows.

Figure 7 shows the corresponding wall pressure distributions. Again, the linear models produce incorrect results, reflecting their problems in representing the flow topology properly.

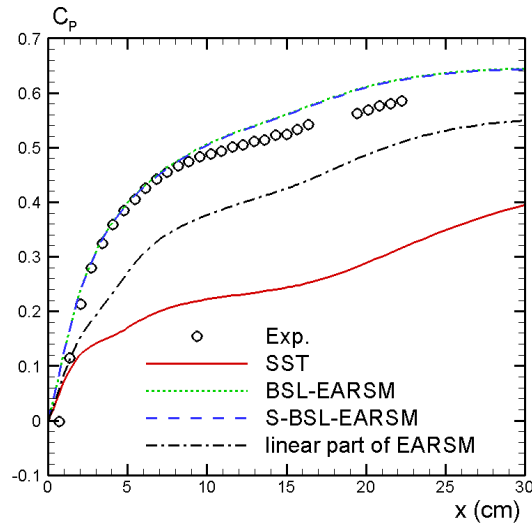


Figure 7: Comparison pressure coefficient for 3D Diffuser

### Transonic flow past DLR F-6 airplane configuration

This test case was first calculated with the SST model using ANSYS-CFX for the 2nd AIAA Drag Prediction Workshop (DPW, 2003) (Langtry et al., 2004). The same simulation setup was used here to compare the S-BSL-EARSM and its isotropic version (activating only  $\beta_l$ ) with the SST model. The variant for the geometry with mounted engine as shown in Figure 8, was selected for comparison, with an angle of attack of 1 degree, providing a lift coefficient of about 0.5. This variant was also used by Peng and Eliasson (2004) to compare the size of separation zones at the 3-D wing-fuselage corner (upper wing surface) and behind the engine (lower wing surface) between the results of several different turbulence models, including SST and EARSM (see also paragraph 20.3.3 in Haase et al., 2006). In Figure 9 these areas of interest are marked by a yellow circle.

Transonic flow calculations at a Mach number of 0.75 and  $Re=3 \times 10^6$  were performed on a block-structured grid of 8.4 million elements. References to the measurement carried out at ONERA are available in (DPW, 2003). In order to evaluate the pure effect of anisotropy of the diagonal Reynolds stresses, one additional simulation was done including only the linear contribution  $\beta_l T_l$  (see Eqs. (1-3)), i.e. using the isotropic part of the model. This is done, as the differences between the  $\beta_l$  contribution and the SST models eddy-viscosity could also change some of the characteristics of the flow in the corner, without any effect of the stress anisotropy. The effect of the anisotropy can therefore best be seen by comparing the S-BSL-EARSM and the  $\beta_l$ -limited variant (it is to be emphasized that the  $\beta_l$ -limited variant is by no means recommended – it is only run to evaluate the impact of the anisotropic part of the EARSM formulation).

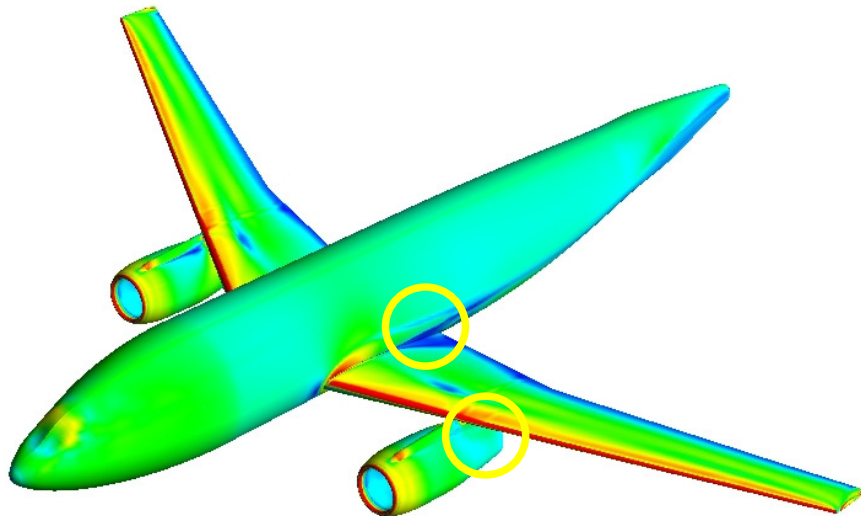


Figure 10: Geometry DLR F6 Wing-Body-Pylon-Nacelle Testcase

As already noticed with the earlier results, the SST model tends to over-predict the size of the corner separation zones, as shown in Figure 11. The S-BSL-EARSM model improves the result for the wing-fuselage corner separation on the upper wing surface (left set of pictures in Figure 11). It is to be noted however, that already the isotropic version ( $\beta_I$ -limited variant) reduces the separation zone somewhat relative to SST. Therefore not the entire effect is a result of the stress anisotropy. Nevertheless, the anisotropic model again significantly improves the solution in this region, resulting in a much improved comparison with the experimental oil flow picture.

The other corner separation zone sits on the lower wing surface behind the engine. It is also over-predicted by the SST model. However, it has fully disappeared in both the S-BSL-EARSM and the  $\beta_I$ -limited EARSM simulations (right set of pictures in Figure 11). This change can therefore not be attributed to the anisotropic representation of the stress-tensor alone. This model behavior will have to be further investigated and is likely a result of elliptic effects changing the flow on a more global level.

For this complex application a reduced robustness of the solver was observed. The time step had to be reduced significantly, resulting in corresponding increase in computing times. This behavior of the model has however not been investigated systematically and needs further investigation.

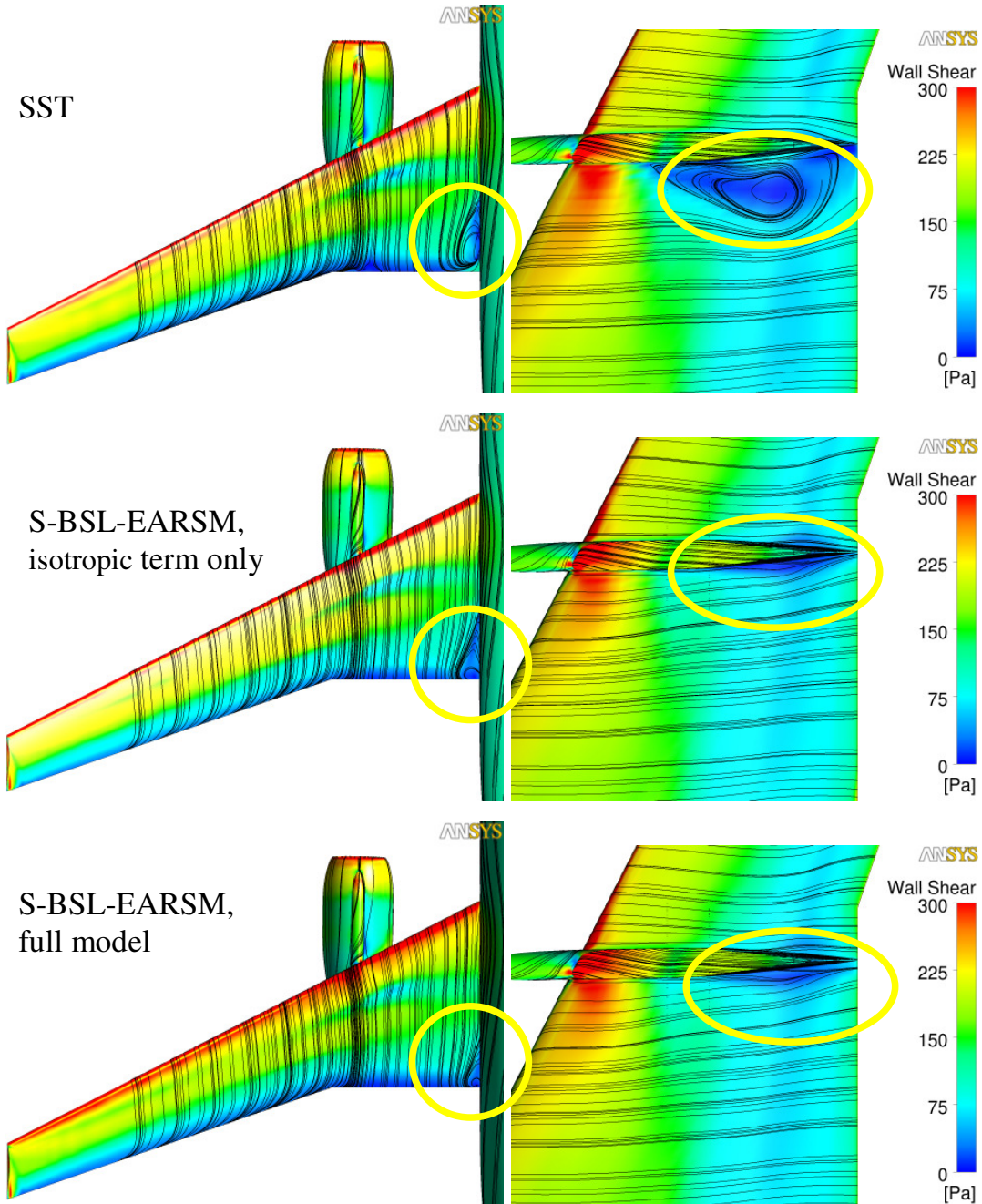
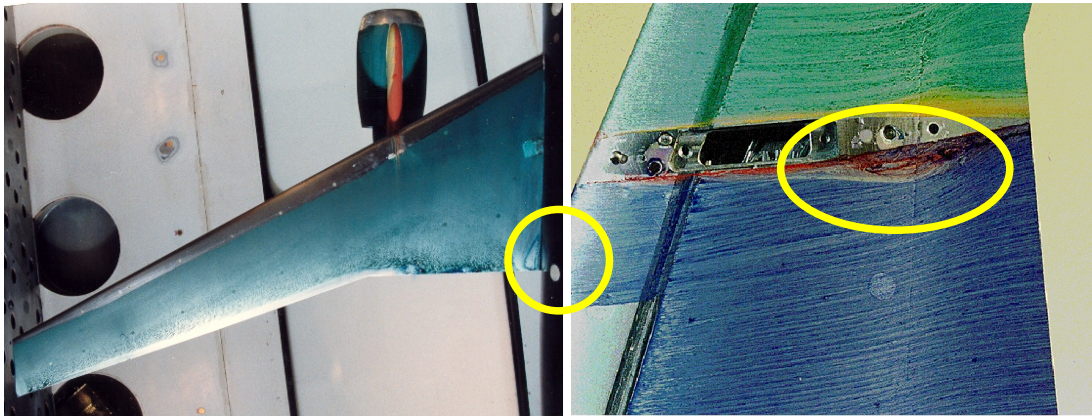


Figure 11: Separation zone at the wing-fuselage junction (left) and behind the engine (right). Top – oil film visualization in the experiment.

## Summary

In the present paper, two variants of EARSM have been presented and applied to a number of testcases. Both formulations start from the WJ EARSM stress-strain relationship. The goal of the first step was to combine the EARSM with the  $\omega$ -equation based BSL model, to avoid freestream sensitivities and ambiguities in comparison with the SST model. This could be achieved by a slight change in the  $A_1$  constant. In addition, the standard eddy-viscosity formulation is used in the diffusion terms of the  $k$ - and the  $\omega$ -equations.

Secondly, a simplified version of the stress-strain relationship was developed. It is based on a linear form of the implicit algebraic model. It is not clear at the time if this formulation possess significant advantages against the WJ stress-strain model. For the current cases both variants produced essentially identical results.

Several testcases have been computed. The flat plate confirms that the model produces correct wall shear stress levels and a proper log. layer. The main interest in the simulations was on corner flow separation. The computation of the 3d Stanford diffuser shows that the inclusion of the stress anisotropy leads to a drastic improvement of the results for this case. The flow topology matches much better the experimentally observed flow and the wall pressure distribution improves significantly. It should however be emphasized that this is a very sensitive flow and that such drastic changes are not to be expected for most engineering applications. Finally, the flow around a wing-bode-pylon-nacelle configuration was simulated. The goal was again a reduction of the corner flow separation. On the upper wing-body intersection, a marked improvement attributed to the anisotropy was observed. On the lower wing-pylon intersection, the results are inconclusive, as they change already when using the isotropic form of the EARSM.

The current tests should be considered as a first iteration in the formulation of improved RANS models for flows with corner separation. Especially numerical robustness and the near wall formulation of the anisotropies will require further optimization. Nevertheless, the results are encouraging and demonstrate the potential of EARSM for such flows.

## Acknowledgment

The authors want to thank Stefan Wallin for his comments during the model formulation.

## References

- Cherry, E.M., Elkins, C.J., and Eaton, J.K., (2007), "Geometric Sensitivity of 3-D Separated Flows", Proc. of 5th International Symposium on Turbulence and Shear Flow Phenomena - TSFP5, Munich, August 27-29, 2007.
- DPW, (2003), 2nd AIAA CFD drag prediction workshop, <http://aaac.larc.nasa.gov/tsab/cfdlarc/aiaa-dpw/>, Orlando, FL., June 21-22, 2003.
- Durbin, P.A., (1991), "Near-wall Turbulence Closure Modeling without "Damping Functions"". Theoretical and Computational Fluid Dynamics, v. 3, N. 1, PP. 1-13.
- Haase, W., Aupoix, B., Bunge, U., Schwamborn, D. (eds), (2006), FLOMANIA – "A European initiative on flow physics modeling – Results of the European-Union funded project 2002-2004". Notes on Numerical Fluid Mechanics and Multidisciplinary Design , Vol. 94, Springer, Berlin/Heidelberg.

- Hellsten A. and Laine, S., (2000), "Explicit Algebraic Reynolds Stress Modelling in Decelerating and Separating Flows", AIAA Paper 2000-2313, Denver.
- Huser, A., Biringen, S., (1993), "Direct numerical simulation of turbulent flow in a square duct", J. Fluid Mech., v. 257, pp. 65-95.
- ERCOFTAC/IAHR (2008) 13<sup>th</sup> workshop on refined turbulence modelling, Sept. 2008. (<http://130.83.243.201/ercofac-sig15/workshop2008.html>)
- Gatski, T.B., and Speziale C.G., (1993) "On explicit algebraic stress models for complex turbulent flows", J. Fluid Mech., 254, 59-78
- Langtry, R.B., Kuntz, M., Menter, F.R., (2004), "Drag prediction of engine-airframe interference effects with CFX-5", AIAA Paper 2004-0391.
- Menter, F.R., (1994), "Two-equation eddy-viscosity turbulence models for engineering applications", AIAA Journal, Vol. 32, No. 8, pp. 1598-1605.
- Menter F.R., (2009), "Review of the shear-stress transport turbulence model experience from an industrial perspective", Int. J. of Comp. Fluid Dynamics, Vol. 23, No. 4, 3005-316.
- Pope, S.B., (1975), "A more general effective-viscosity hypothesis", J. Fluid Mech., 72, pp. 331-340.
- Peng, S., Eliasson, P. (2004) A comparison of turbulence models in prediction of flow around the DLR-F6 aircraft configuration, AIAA Paper 2004-4718, 22nd AIAA Applied Aerodynamics Conf., Providence, Rhode Island, 16-19 August 2004.
- Rodi, W., (1976), "A new algebraic relation for calculating the Reynolds stresses", Z. Angew. Math. Mech, Vol. 56, pp 219-221.
- Strelets, M., 2001, Detached-Eddy Simulation of Massively Separated Flows, AIAA Paper 2001-0879.
- Wallin, S., (2009), Personal communication.
- Wallin, S., Johansson, A.V., (1997), "A new explicit algebraic Reynolds stress turbulence model for 3D flow", Proceedings of the 11th Symposium on Turbulent Shear Flows, Grenoble, France. v.2, p. 13.
- Wallin, S. and Johansson, A.V., (2000), "An explicit algebraic Reynolds stress model for incompressible and compressible turbulent flows", J. Fluid Mech., 403, pp. 89-132.
- Wieghardt, K., and Tillmann, W., (1951), "On the turbulent friction layer for rising pressure", NACA TM 1314.